Technical Paper

ISSN 1997-1400 Int. J. Pavement Res. Technol. 7(5):352-360

Modeling of the Asphalt Concrete to Compare Uniaxial, Hollow Cylindrical, and Indirect Tensile Test

Sanjeev Adhikari[1], Hainian Wang[2+], Zhanping You[3], Gregory M. Odegard[4], and Peiwen Hao[2]

Abstract: The objective of this study is to develop a micromechanical based Discrete Element Model (DEM) to simulate dynamic modulus of the asphalt concrete using Uniaxial Tensile (UT), Hollow Cylindrical Tensile (HCT), and Indirect Tensile (IDT) model. This research is used to compare DEM simulation of the UT, HCT, and IDT tests. The asphalt concrete mixture used was a 19 mm Nominal Maximum Aggregate Size (NMAS) with an asphalt content of 5.59% and air void level of 4.36% to develop UT, HCT, and IDT model. The dynamic moduli of the sand mastic and stiffness of aggregate were used as input parameters of the DEM to predict the dynamic moduli of the asphalt concrete through a virtual testing of UT, HCT, and IDT. The sand mastic had an NMAS of 1.18mm, which was used in a DEM. The three-dimensional (3D) internal microstructure of the asphalt concrete mixture (i.e., distribution of aggregate, mastic, and air voids) was obtained through the X-ray CT (Computed Tomography). From the 3D X-ray CT images, location of aggregates, mastic, and air voids were obtained using image processing. The laboratory measured dynamic moduli of asphalt concrete were used to compare predicted dynamic moduli of UT, HCT, and IDT tensile models. It was found that the UT model was able to predict the asphalt concrete modulus across a range of temperatures and loading frequencies. The HCT model was slightly lower at low and high temperatures, and the IDT model was slightly higher at a low temperature and slightly lower at high temperature. The results indicate that UT, HCT, and IDT tensile are useful models to predict dynamic moduli of asphalt concrete.

DOI: 10.6135/ijprt.org.tw/2014.7(5).352

***Key words**: Asphalt concrete, Hollow Cylindrical Test, Indirect Tensile Test, Image processing, Microstructure, Uniaxial Test, X-ray CT.*

Introduction

Microstructure based micromechanical models predict the dynamic modulus of asphalt concrete based upon the properties of individual constituents, such as the mastic, aggregate, and air void. The micromechanical model of discrete element is used to predict the dynamic moduli of the asphalt concrete through a virtual testing of UT, HCT, and IDT. Micromechanical models were developed for different composite materials [1-8]. Many studies have shown that the traditional micromechanical models do not adequately describe the complex microstructure of the asphalt mixture. The discrete element method is a good technique for micromechanical modeling of the asphalt concrete microstructure. The discrete element method was initially developed by Cundall [9-12]. Cundall used the discrete element method to model soil or rock mass under loading to get the geomechanics response. Fault development of the rock mass was also modeled using the discrete element method. Rottenberg [13] used the discrete element model to evaluate rutting by considering the angular particles of aggregate in an asphalt concrete.

The mechanical properties of asphalt concrete specimen were predicted by Buttlar and You [14] using the micromechanical based Discrete Element Model (DEM). They used PFC2D code to predict creep strains and modulus of an asphalt concrete subjected to diametral loads in the indirect tension test. Collop et. al. [15] applied a discrete element method to investigate the mechanical behavior of idealized asphalt concrete. The possibilities of initial elastic, visco-elastic, and visco-plastic behavior prediction were stated using DEM simulation. You and Buttlar [16] used a two-dimensional linear elastic DEM to simulate complex moduli of asphalt concrete.

The comparison of two dimensional (2D) and three dimensional (3D) micromechanical discrete element simulation was developed by You et al [17]. Adhikari and You [18] predicted the asphalt concrete dynamic modulus using 2D and 3D DEM generated from the X-ray computed tomography (X-ray CT) images. It was found that the 3D discrete element models were able to predict the concrete moduli considering air void distribution. The X-ray tomography imaging technique has been used increasingly in asphalt material in recent years. X-ray CT has the advantage of acquiring the internal microstructure with high accuracy [19]. Shashindhar [20] and Masad et al [21] used X-ray CT images to study the compaction of asphalt concretes. You et al [22] studied the microstructure of the asphalt concrete due to the air void effect under laboratory and field compaction patterns on asphalt mixtures. They also investigated the air void effect from X-ray CT images. The air void distribution in laboratory-compacted specimens usually

[1] Department of Applied Engineering and Technology, Morehead State University, 301 Lloyd Cassity, Morehead, Kentucky 40351, USA.

[2] Key Laboratory for Special Area Highway Engineering of Ministry of Education, Chang'an University, Xi'an, 710064, China.

[3] Department of Civil and Environmental Engineering, Michigan Technological University, 1400 Townsend Drive, Houghton, Michigan, 49931-1295, USA.

[4] Department of Mechanical Engineering - Engineering Mechanics, Michigan Technological University, Houghton, Michigan, 49931, USA.

[+] Corresponding Author: E-mail s.adhikari@moreheadstate.edu

Note: Submitted June 19, 2013; Revised July 14, 2014; Accepted July 16, 2014.

followed a “C” shape. The air void distribution in the field cores was concentrated at the bottom of the specimens. Adhikari et al [23] studied multiphase characterization of asphalt concrete using X-ray microfluorescence.

You et al [24] presented a real 3D microstructure model of the aggregates-mastic-air system captured with the X-ray computed tomography (CT) method, a non-destructive 3D image acquisition technique. It was found that the 3D discrete element model from the X-ray CT image successfully predicted the mixture modulus across a range of temperatures and loading frequencies. Adhikari and You [25] investigated the sensitivity of the aggregate size in sand mastic using microstructure modeling from the X-ray CT image of the asphalt concrete. Three different types of sand mastic were chosen with Nominal Maximum Aggregate Size (NMAS) of 1.18mm, 0.6mm, and 0.3mm. The sand mastic of 0.6mm NMAS accurately predicted the asphalt mixture dynamic modulus across a range of temperatures and loading frequencies. The asphalt concrete model using NMAS of 1.18mm sand mastic was slightly under-predicted because of an absence of a smaller aggregate size and interaction of larger aggregate size only in the asphalt mixture model. The asphalt concrete model using NMAS of 0.3 mm sand mastic was slightly over-predicted. Adhikari and You [26] used a hollow cylindrical model with an X-ray tomography image to reconstruct the assembly of discrete element models. The moduli of the 3D models were then compared with 2D models and the experimental data. The modulus prediction of 3D DEM was around 27% higher than that of the 2D model. The experiment based viscoelastic behavior was incorporated into the DEM. The Burger’s contact model was used in the sand mastic phase during the viscoelastic simulation. When comparing the lab measurements with the elastic and viscoelastic simulations, the dynamic modulus of lab measurements were higher than the elastic and viscoelastic simulation.

In this study, 3D DEM was used to simulate dynamic modulus of the asphalt concrete using Uniaxial Tensile (UT), Hollow Cylindrical Tensile (HCT), and Indirect Tensile (IDT) test. Three-dimensional (3D) internal microstructure of the asphalt concretes (i.e., distribution of aggregate, mastic, and air voids) was obtained through the X-ray CT. From the 3D X-ray CT images, the location of aggregates, mastic, and air voids were obtained using image processing. The DEM simulation of the UT, HCT, and IDT test was also compared in this paper. Sand mastic dynamic modulus was used as an input parameter in the 3D DEM. The laboratory measured dynamic moduli of asphalt concrete were used to compare predicted dynamic moduli of three different tensile models. The Particle Flow Code (PFC) was used in the discrete element modeling prediction. The modulus from the prediction was compared with the laboratory measured asphalt concrete dynamic modulus.

Objective and Scope

The objectives of this study are: 1) to develop 3D micromechanical discrete element models to simulate the modulus of an asphalt concrete using UT, HCT, and IDT tests; 2) to compare the dynamic modulus prediction from different testing methods. This study uses a DEM to predict the dynamic modulus of the asphalt specimens using the heterogeneous microstructures visualized from X-ray CT images. An asphalt concrete model is divided into aggregate, sand mastic, and air void phases on the modeling. Sand mastic had a maximum aggregate size of 1.18 mm. The modeling approach used was the 3D DEM approach. The asphalt concrete modulus was predicted by using aggregate and mastic stiffness.

Mechanical Response of Different Tensile Tests

This section briefly discusses mechanical response of UT, HCT, and IDT models of an asphalt concrete. Fig. 1 shows the development of three different tensile models of the asphalt concrete. UT model and HCT model were developed by cutting the inner and outer core of the asphalt concrete. The IDT model was developed from cross sectional horizontal cutting of the asphalt concrete. The dimensions of the asphalt concrete were 150 mm in diameter and 150 mm in height. The asphalt concrete was cored into a diameter of 100 mm and a height of 150 mm to get the UT model. The HCT model had outer diameter of 150 mm, inner diameter of 100 mm, and height of 150 mm. The dimensions of the IDT specimen were 150 mm in diameter and 50 mm in height.

Hollow Cylindrical Tensile Test

The principle behind the HCT test is to apply internal pressure to the inner cavity of the hollow cylinder specimen. The circumference pressure and longitudinal stress is developed on the hollow cylinder specimen due to the internal pressure. Haven and Swett [27] described the maximum intensity of circumference stress at the inner surface by the following equation:

$$\sigma_r = p\left(\frac{R_2^2 + R_1^2}{R_2^2 - R_1^2}\right) \tag{1}$$

and for the outer surface

$$\sigma_r = p\left(\frac{2R_1^2}{R_2^2 - R_1^2}\right) \tag{2}$$

where, R_2 and R_1 are the outer radius and inner radius, respectively. The radial strain at the surface of the hollow specimen can be calculated as

$$\varepsilon_r = \frac{\Delta r}{r} \tag{3}$$

The modulus of the hollow cylinder can be calculated as

$$E = \frac{\sigma_r}{\varepsilon_r} = \frac{p \cdot \Delta_{R1}}{R_1}\left(\frac{R_2^2 + R_1^2}{R_2^2 - R_1^2}\right) \tag{4}$$

Alavi and Monismith [28] used the HCT test to determine the shear and compressive properties of asphalt concrete. Buttlar et al. [29] and Al-khateeb [30] developed an HCT test device to determine the mechanical properties of the asphalt concrete. They measure dynamic modulus by applying the different loading frequencies in the inner surface of the cylinder.

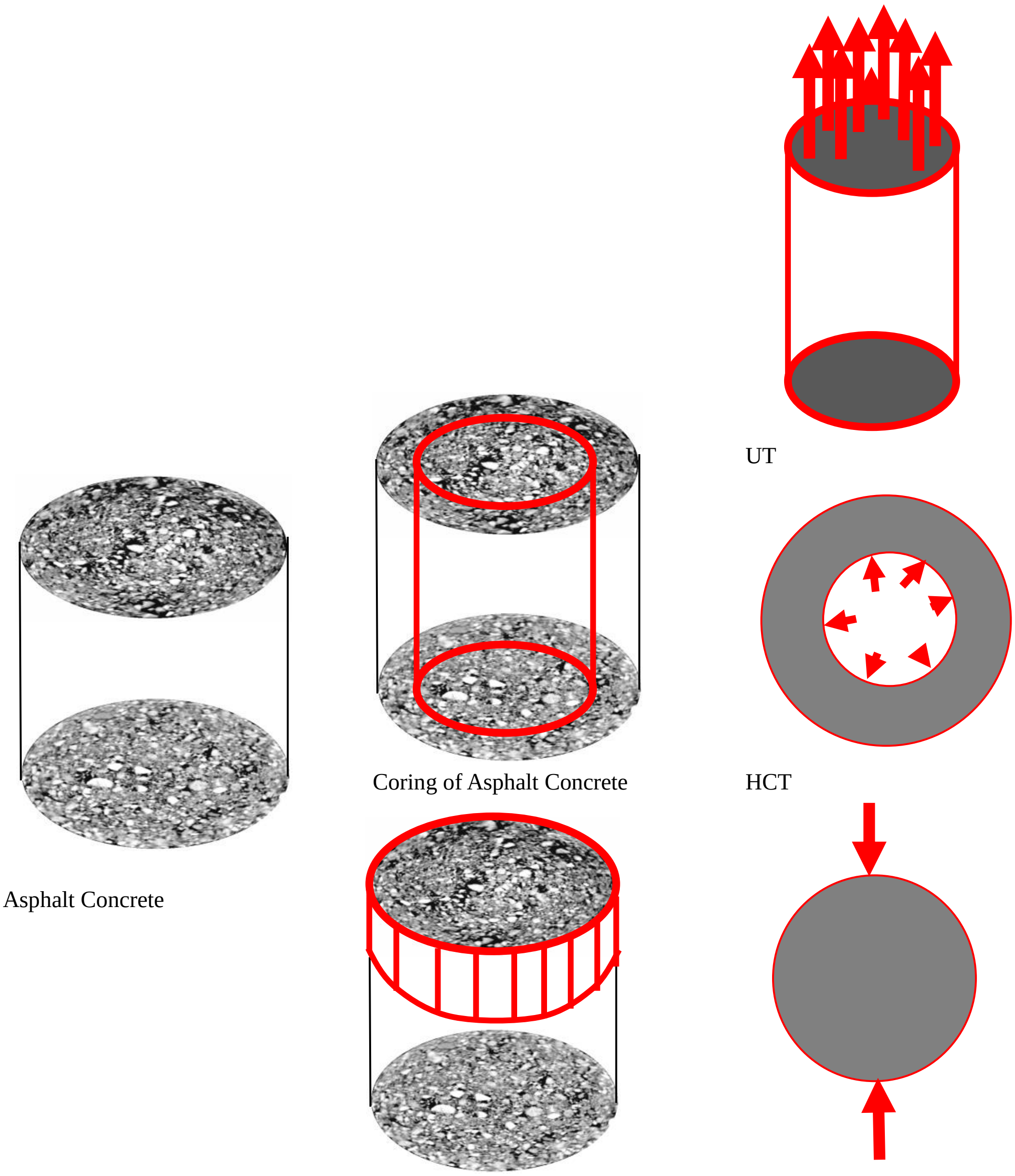

Fig. 1. Development of Three Different Tensile Models.

Indirect Tensile Test

The indirect tensile test is conducted by subjecting a uniform diametric pressure, p, along the top surface as shown in Fig. 2. The tensile stress and compressive stress are developed inside specimen due to the diametric pressure. The tensile and compressive strains are produced due to corresponding stress on the specimen. Kaklis et al. [31] described tensile stress at the specimen by the following equation:

$$\sigma_t = \frac{2P}{\pi Dt} \tag{5}$$

and compressive stress at specimen by following equation:

$$\sigma_c = \frac{6P}{\pi Dt} \tag{6}$$

where, D and t are the diameter and thickness of spacemen respectively.

The corresponding strain $\varepsilon_t, \varepsilon_c$ at the specimen is calculated from the change in displacement. That strain is used to calculate modulus of elasticity. The equation of modulus of elasticity is calculated as:

$$E = \frac{\sigma_t}{\varepsilon_t} \tag{7}$$

Uniaxial Tensile Test

The universal tensile test is conducted by applying tensile pressure on the top and bottom of the cylindrical specimen along the axial direction. The tensile stress and tensile strains are developed on the

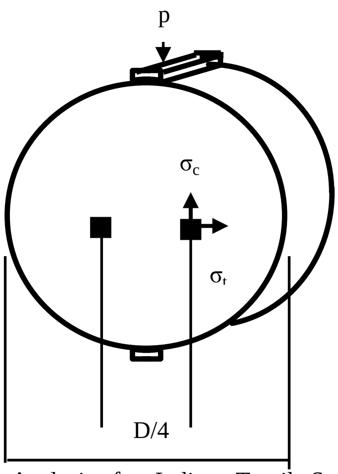

Fig. 2. Analysis of an Indirect Tensile Specimen.

cylinder specimen due to the external pressure. The modulus was calculated by dividing tensile stress by tensile strain. Tensile stress of the specimen is given by the equation

$$\sigma_t = \frac{P}{A} \tag{8}$$

where P is tensile force and A is the cross section area of specimen.

The corresponding strain ε_t is calculated from the change in displacement due to loading. Dynamic modulus is determined by the following equation:

$$E = \frac{\sigma_t}{\varepsilon_t} \tag{9}$$

Laboratory Tests

Asphalt concretes specimen were prepared using 5.57% asphalt content of PG 64-28 grade and compacted to 4.36% air voids using a Superpave gyratory compactor. The aggregate used in this study was a 12.5 mm nominal maximum aggregate size mix. Dynamic modulus of sand mastic and aggregate modulus were used as an input to predict mixture modulus. In order to measure the aggregate modulus needed for the DEM simulation, stone cylinders were cored and cut from large boulders. The aggregate specimen had a diameter of 70 mm and a height of 150 mm. An aggregate modulus of 55.5 GPa was used in the models. Dynamic modulus was measured from universal axial testing machine. The nominal maximum aggregate size of sand mastic was 1.18 mm. Table 1 shows the aggregate gradations of the asphalt mixture and the sand mastic used in this study. The asphalt content in the sand mastic was around 10.33%.

The dynamic modulus of the sand mastic was measured through uniaxial compressive tests. The dynamic modulus test of asphalt mixture had a diameter of 100 mm and a height of 150 mm, which had been cored and cut from gyratory compacted specimens that were 150 mm in diameter and 165 mm in height. The sand mastic specimen had a diameter of 75 mm and height of 150 mm, which was obtained by trimming the ends of a 190 mm tall specimen extracted from the 75 mm diameter mold. The dynamic modulus of

Table 1. Aggregate Gradation for Asphalt Mixture and Sand Mastic Tested in Dynamic Modulus Test (Percent Passing)

Sieve Size (mm)	Nominal Maximum Aggregate Size, mm (Percentage Passing)	
Sieve Size (mm)	Asphalt Mixture 12.5	Sand Mastic 1.18
19	100	100
12.5	98.7	100
9.5	86.5	100
4.75	71.8	100
2.36	51.4	100
1.18	36.1	70.23
0.6	25.5	49.61
0.3	14.7	28.6
0.15	7.7	14.98
0.075	5.4	10.51
Asphalt Content	5.59	10.33
Air Voids (%)	4.36	0*

*Air voids were zero for the sand–mastic slurry materials with high asphalt content.

Sand mastic 1.18mm Asphalt concrete

Fig. 3. Asphalt Concrete and Sand Mastic.

the asphalt mixture was predicted using the DEM model and by the sand mastic dynamic modulus and aggregate modulus. Fig. 3 shows snapshots of sand mastic and asphalt concrete specimens. The dynamic modulus of both the sand mastic and asphalt concretes was tested across a range of loading frequencies (0.1 Hz, 0.5 Hz, 1 Hz, 5 Hz, 10 Hz, and 25 Hz) and test temperatures (4^{o}C, -6^{o}C, and -18^{o}C). The dynamic modulus measurements of asphalt concrete were compared with the discrete element modeling of asphalt concrete.

Image Processing of X-ray CT Images

The 3D internal structure of the asphalt mixture (i.e., spatial distribution of aggregate, mastic, and air voids) was acquired using the X-ray Computed Tomography (CT) imaging technique. X-ray CT is a non-destructive imaging technology that is capable of providing a 3D image of the internal structure of a solid object. The X-ray CT technique was used to provide geometric information to represent asphalt concrete for the DEM simulations. 3D X-ray CT image of asphalt concrete was used to obtain locations (coordinates) of aggregates, mastic, and air voids. Image processing was conducted based on their gray scale intensities that ranged from 0 to 255. In general, dense materials such as aggregates are shown with brighter pixels (close to 255), whereas air voids with negligible density are seen with dark pixels (close to 0). The mastic has an

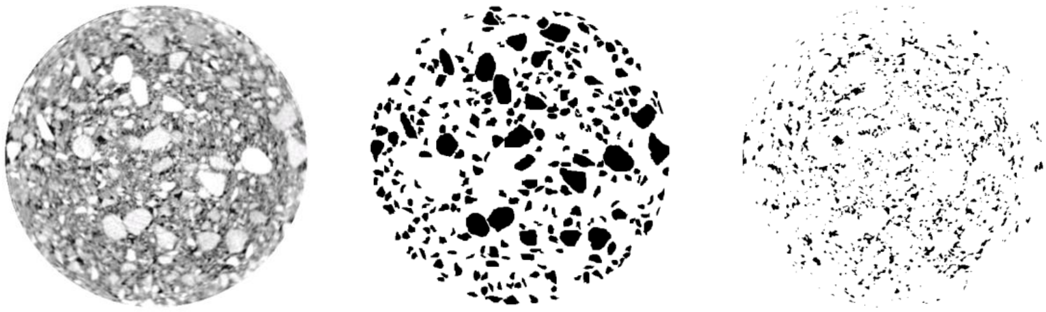

Fig. 4. Illustration of Gray Images Acquired by X-ray CT with Air Void and Aggregate Size Distribution of 1.18 mm in a 2D Space.

intermediate density on gray color. An image processing technique was used to transfer X-ray gray image into aggregate, mastic, and air voids images according to a threshold segmenting of each element. Fig. 4 shows the segmentation to separate air voids, aggregate, and mastic domain. Aggregate size larger than 1.18 mm is shown in Fig. 4. The separation of the mastic threshold index was determined by volumetric analysis. The air void level index was chosen as 0-124. The threshold index of an aggregate size larger than 1.18 mm was selected as 202-255. The mastic and aggregate threshold were chosen from the volume of mastic and aggregate used in the mixture.

Discrete Element Modeling

The asphalt concrete is a heterogeneous material of coarse aggregate, sand mastic, and air voids. The asphalt concrete microstructure was captured using X-ray tomography. Image processing techniques were used to identify the aggregate, mastic, and air voids from the X-ray CT images. The mastic was finer than 2.36 mm in the X-ray image. The assembly of horizontal slices of X-ray CT images was reconstructed to form a cylindrical specimen. The image consists of 256 levels of gray intensity. The gray images of X-ray CT images were transferred into aggregate, mastic, and air void images according to a threshold segmenting of each element. Aggregate, mastic, and air void images were input into DEM by using discrete balls of 0.5 mm radius. Three types of DEM were generated in this study. Cylindrical-shaped models were prepared for UT tests and IDT tests. A hollow cylindrical-shape was prepared for the HCT test. Fig. 5 illustrates the extraction of HCT, UT, and IDT models developed from the cylindrical asphalt specimen, where the aggregates, mastics, and air voids are easily seen. The radius of each sphere was 0.5 mm for all models.

The 3D hollow cylinder was used with an outer diameter of 150 mm, inner diameter of 100 mm, and depth of 150 mm in the DEM simulation. There were a total of 487,200 spheres in the 3D asphalt concrete model. The aggregate volume was calculated by dividing the number of aggregate elements by the number of total elements, which was around 31.27%. The air voids were around 6.76%. The dimensions of the uniaxial cylindrical DEM were 100 mm in diameter and 150 mm in height. There were a total of 404,460 spheres in this 3D asphalt concrete DEM. There was a total of 49.73% aggregate phase of DEM. The air voids were around 1.65%. The 3D IDT cylinder specimen was used with diameter of 150 mm and depth of 50 mm in the DEM simulation. There was a total of 296,240 spheres in this 3D asphalt concrete model. The aggregate volume was around 38.79%. The air voids were around 4.72%. Air void content was considered on the model. The gyratory compaction specimen had higher air void in the outer periphery and lower air void in the inner periphery.

The air void elements were deleted in the DEM. A 3D discrete element model was constructed using closed-packing cubic arrays of spheres. The closed-packing arrays are based upon the face-centered packing spheres [32]. The 3D DEMs were used to predict the dynamic modulus of the asphalt concrete. The sand mastic's dynamic modulus and aggregate's modulus were input into the DEM to predict the asphalt concrete modulus.

The modulus of the hollow cylindrical asphalt model was simulated with 3D DEM by applying tensile stress on the inner surface of the hollow cylinder. The strains in the radial directions were computed using the change in displacement on the inner surface. The modulus was computed from the plots of radial stress versus radial strain. The modulus of the uniaxial tensile model was simulated by applying tensile stress at the top and bottom surfaces of the cylindrical model. The tensile strains in the axial direction were computed using the change in displacement on the top surface of the cylinder. The modulus was computed from the plots of tensile stress versus tensile strain.

The modulus of the IDT model was simulated by applying compressive stress at the diametric section of the cylindrical model. The tensile stresses and strains at the center of the cylindrical specimen were calculated. The modulus was computed from the tensile stress divided by tensile strain. The contact stiffness model was used in the contact of discrete balls. The contact stiffness model provides an elastic relationship between the contact force and relative displacement between particles. The interaction of aggregates and mastics, mastics and mastics, and aggregate and aggregate were prepared with a linear contact stiffness model. For a linear contact model, the contact stiffness is computed by assuming that the stiffness of the two contacting entities acts in series. The force-displacement law of the two elements in contact can be represented using different constitutive laws.

Results of DEM

The dynamic modulus prediction of the asphalt concrete using UT, HCT, and IDT discrete element models is presented in this section. The 3D DEM simulations' modulus results were compared with the experimental measurements to evaluate the accuracy of the different

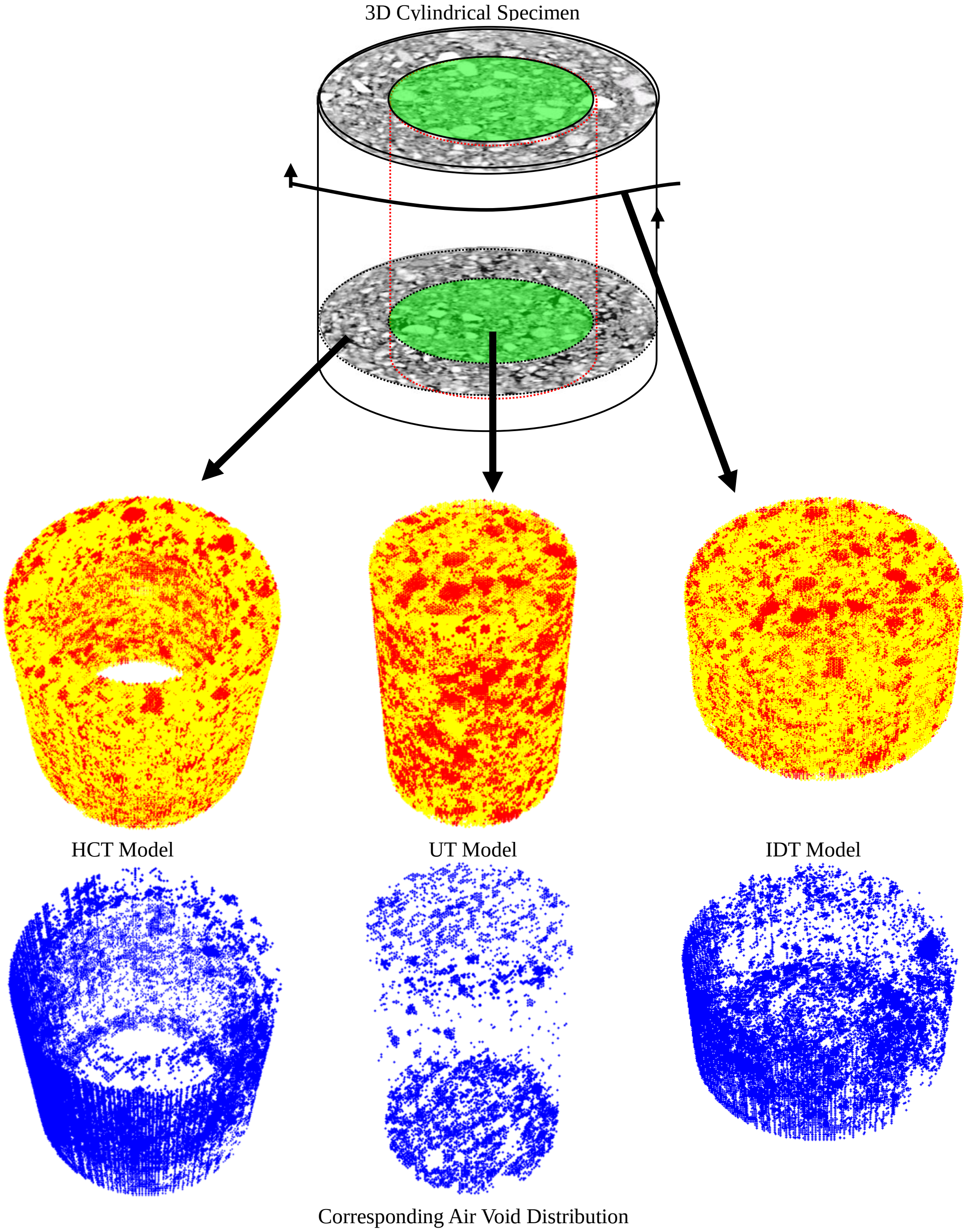

Fig. 5. Demonstration of 3D DEM.

simulation methods. The dynamic modulus of the asphalt mastic across a range of loading frequencies (0.1 Hz, 0.5 Hz, 1 Hz, 5 Hz, 10 Hz, and 25 Hz) and test temperatures (4^{o}C, -6^{o}C, and -18^{o}C) were measured. The moduli of sand mastic 1.18 mm were used as input parameters in the asphalt concrete models.

The 3D discrete element models of the asphalt concrete of UT, HCT, and IDT were evaluated. 3D models yielded a better prediction on the mixture modulus. The asphalt mixture was compacted to a 4.36% air void level. Different air void levels were calculated on UT, HCT, and IDT during modeling. The air voids of UT, HCT, and IDT were around 1.65%, 6.76%, and 4.72% respectively. The asphalt cylindrical specimen had more air void on outer periphery than inner core. Asphalt specimen was more compacted inside than outer periphery of specimens.

The 3D DEM simulations' moduli were compared with the measurements to evaluate the accuracy of the different simulation methods. The dynamic moduli, E*, of the asphalt mastic over a range of loading frequencies (0.1 Hz, 0.5 Hz, 1 Hz, 5 Hz, 10 Hz, and 25 Hz) and test temperatures (4^{o}C, -6^{o}C, and -18^{o}C) were measured and used as input parameters in the 3D discrete element models. Therefore, at each loading frequency and test temperature, the prediction of the asphalt mixture modulus was obtained to simulate the 3D DEMs. The asphalt mixture modulus predictions from the UT, HCT, and IDT models and lab measurements are shown in Figs. 6, 7, and 8 respectively, over a range of loading frequencies and test temperatures.

A comparison of dynamic modulus prediction using the UT model, the HCT model, and the IDT model with the experimental measurements (from three temperatures and six loading frequencies) is shown in Fig. 9. The 3D DEM prediction using the UT model and the IDT model was very close to the asphalt concrete's modulus measurements. The modulus of 3D DEM using HCT was under-predicted. The HCT model was under-predicted at low and high temperature and the IDT model slightly over-predicted at a low temperature and slightly under-predicted at high temperature. The HCT model was slightly lower at low and high temperatures. The dynamic modulus prediction of UT model and IDT models are very close to laboratory measurements. It was found that for each temperature and frequency, the prediction is very close to the asphalt mixture modulus measurements at UT and IDT model. The results indicate that UT, HCT, and IDT tensile models are used to predict dynamic moduli of asphalt concrete.

Summary and Conclusion

The asphalt concrete was simulated with the Uniaxial Tensile (UT), Hollow Cylindrical Tensile (HCT), and Indirect Tensile (IDT) test to compare dynamic modulus. The 3D morphology of the asphalt concrete mixture was captured with an X-ray tomography image and reconstructed into the assembly of discrete element models. The dynamic moduli of the sand mastic and modulus of aggregate were used in the discrete element models. The dynamic moduli of the asphalt concrete were used to assess the discrete element models. The predicted dynamic modulus from a DEM at frequencies of 0.1 Hz, 0.5 Hz, 1 Hz, 5 Hz, 10 Hz, and 25 Hz and test temperatures of 4°C, -6°C, and -18°C were compared on the model. It was found that the UT model was able to predict the asphalt concrete modulus across a range of temperatures and loading frequencies. The UT model has better prediction because it is an extracted model from the inner portion of Gyratory compaction asphalt specimen. This model has compacted well with aggregate and binder with air void similar to the experimental specimen. The modulus HCT model's prediction was slightly lower at low and high temperatures, and the IDT model's prediction was slightly higher at a low temperature and under-predicted at high temperature. The results indicate that UT,

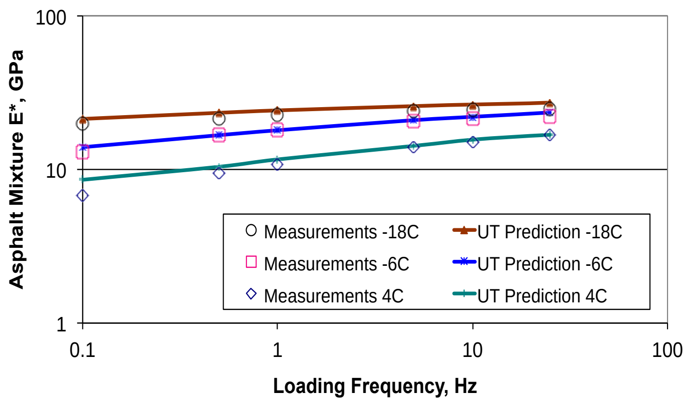

Fig. 6. Comparing Modulus Prediction Using UT Model and Laboratory Measurements of the Asphalt Mixture (from Different Loading Frequencies and Test Temperatures).

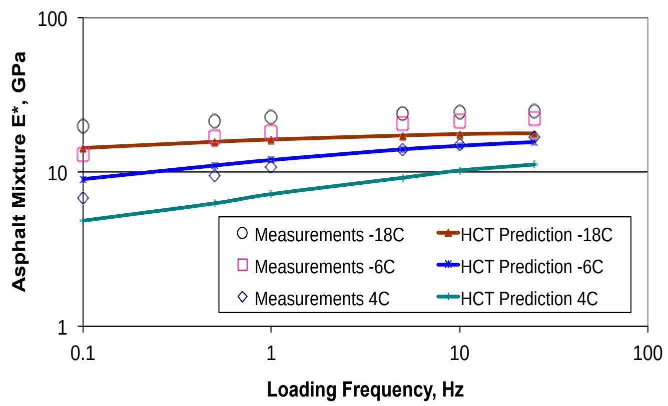

Fig. 7. Comparing Modulus Prediction Using HCT Model and Laboratory Measurements of the Asphalt Mixture (from Different Loading Frequencies and Test Temperatures).

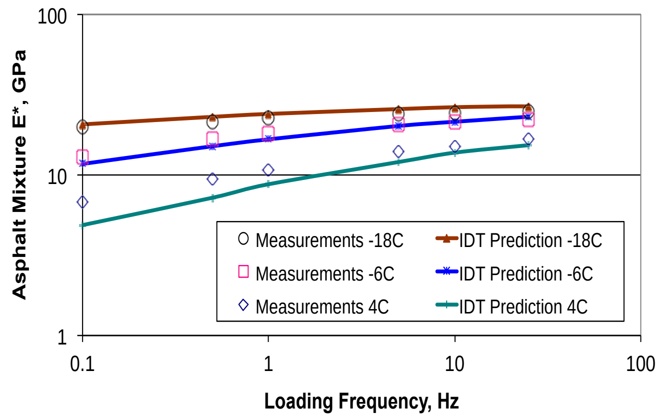

Fig. 8. Comparing Modulus Prediction Using IDT Model and Laboratory Measurements of the Asphalt Mixture (from Different Loading Frequencies and Test Temperatures).

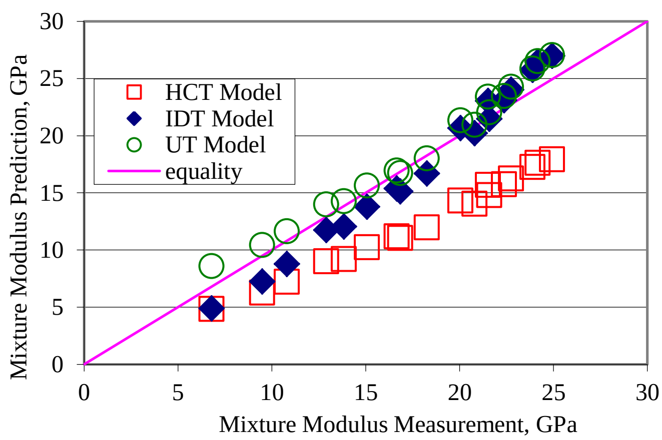

Fig. 9. Three Different Discrete Element Model Comparisons with Lab Measurement.

HCT, and IDT tensile models can be used to predict dynamic moduli of asphalt concrete. Future work will involve the development of the viscoelastic material constitutive models at several temperatures and loading frequencies using the 3D DEM.

Acknowledgements

This material is based in part upon work supported by the National Natural Science Foundation of China (51250110077). Any opinions, findings, and conclusions or recommendations expressed in this material are those of the author's and do not necessarily reflect the views of the National Natural Science Foundation of China.

References

1. Christensen, D.W., Pellien, T., and Bonaquist, R.F. (2003). Hirsch Models for Estimating the Modulus of Asphalt Concrete, *Journal of the Association of Asphalt Paving Technology*, 72, pp. 97-121.
2. Christensen, R.M. and Lo, K.H. (1986). Solutions for Effective Shear Properties in Three Phase Sphere and Cylinder Models, *Journal of the Mechanics and Physics of Solids*, 27, pp. 315-330.
3. Counto, V.J. (1964). The Effect of the Elastic Modulus of the Aggregate on the Elastic Modulus, Creep, and Creep Recovery of Concrete, *Magazine of Concrete Research*, 62(48), pp. 129-138.
4. Hashin, Z. (1962). The Elastic Moduli of Heterogeneous Materials, *Journal of Appied. Mechanics*, 29E, 143.
5. Hashin, Z. (1965). Viscoelastic Behaviour of Heterogeneous Media, *Journal of Applied Mechanics*, Trans, ASME, 9, pp. 630-636.
6. Hirsch, T.J. (1962). Modulus of Elasticity of Concrete Affected by Elastic Moduli of Cement Paste Matrix and Aggregate, *Journal of the American Concrete Institute*, 59(3), 427-452.
7. Kerner, E.H. (1956). The Elastic and Thermo-elastic Properties of Composite Media, *Proceedings of the Physical Society Section B*, 69, 808-813.
8. Tanaka, K., and Mori, T. (1973). Strength-differential Effect in Single Crystal of Martensite, *Scripta Metallurgica*, 7(3), pp. 307-310.
9. Cundall, P.A. (2000). A Discontinuous Future for Numerical Modelling in Geomechanics, *Proceedings of the Institution of Civil Engineers - Geotechnical Engineering*, 149(1), pp. 41-47.
10. Cundall, P.A. (1990). Numerical Modelling of Jointed and Faulted Rock, *Proceedings of the International Conference on Mechanics of Jointed and Faulted Rock*, pp. 11-18.
11. Cundall, P.A. (1987). *Distinct Element Models of Rock and Soil Structure, Analytical and Computational Methods in Engineering Rock Mechanics,* Chapter 4: Brown, E.T. (Ed.), George Allen and Unwin, London, UK, pp. 129-163.
12. Cundall, P.A. (1971). A Computer Model for Simulating Progressive Large Scale Movements in Blocky Rock Systems, *Proceedings of the Symposium of the International Society of Rock Mechanics*, II-8, pp. 129-136.
13. Buttlar, W.G. and You, Z. (2001). Discrete Element Modeling of Asphalt Concrete: A Micro-Fabric Approach, *Transportation Research Record*, No. 1757, pp. 111-118.
14. Collop, A.C., McDowell, G.R., and Lee, Y. (2004). Use of the Distinct Element Method to Model the Deformation Behavior of an Idealized Asphalt Mixture, *International Journal of Pavement Engineering*, 5, pp. 1-7.
15. You, Z. and Buttlar, W.G. (2006). Micromechanical Modeling Approach to Predict Compressive Dynamic Moduli of Asphalt Mixture Using the Distinct Element Method, *Transportation Research Record*, No. 1970, pp. 73-83.
16. You, Z, Adhikari, S., and Dai, Q. (2008). Three-Dimensional Discrete Element Models for Asphalt Mixtures, *Journal of Engineering Mechanics*, 134(12), pp. 1053-1063.
17. Adhikari, S. and You, Z. (2008). 3D Microstructural Models for Asphalt Mixtures Using X-Ray Computed Tomography Images, *International Journal of Pavement Research and Technology*, 1(3), pp. 94-99.
18. Lee, X. and Dass, W.C. (1993). *Experimental Study of Granular Packing Structure Changes under Load,* Elsevier Science Publishers B.V., Amsterdam, Neth, Birmingham, UK, pp. 17.
19. Shashidhar, N. (1999). X-ray Tomography of Asphalt Concrete, *Transportation Research Record*, No. 1681, pp. 186-192.
20. Masad, E., Muhunthan, B., Shashidhar, N., and Harman, T. (1999). Quantifying Laboratory Compaction Effects on the Internal Structure of Asphalt Concrete, *Transportation Research Record*, No. 1681, pp. 179-185.
21. You, Z., Adhikari, S., Masad, E., and Dai, Q. (2009). Microstructural and Micromechanical Properties of Field and Lab-compacted Asphalt Mixtures, *Journal of Association of Asphalt Paving Technologists*, 78, pp. 279-316.
22. Adhikari, S., You, Z. and Peterson, K., (2013). Multi-Phase Characterization of Asphalt Concrete using X-ray Microfluorescence, *International Journal of Pavement Research and Technology*, 6(2), pp. 117-122.
23. Adhikari, S. and You, Z. (2010). The Sensitivity of Aggregate Size within Sand Mastic to Model the Microstructure of Asphalt Mixture. *Journal of Materials in Civil Engineering*, doi:10.1061/(ASCE)MT.1943-5533.0000212
24. You, Z., Adhikari, S., and Kutay, M.E. (2008). Dynamic Modulus Simulation of the Asphalt Concrete Using the X-Ray Computed Tomography Images, *Materials and Structures*, 42(5), pp. 617-630.
25. Adhikari, S. and You, Z. (2010b). 3D Discrete Element Models of the Hollow Cylindrical Asphalt Concrete Specimens Subject to the Internal Pressure, *International Journal of Pavement Engineering*, 11(5), pp. 429–439
26. Haven, G.B., and Swett, G.W. (1915). *The Design of Steam Boilers and Pressure Vessels,* John Wiley and Sons. Inc., New York, USA.
27. Alavi, S.H., and Monismith, C.L. (1994). Time and Temperature Dependent Properties of Asphalt Concrete Mixes Tested as Hollow Cylinders and Subjected to Dynamic Axial and Shear Loads, *Journal of the Association of Asphalt Paving Technologists*, 63, pp. 152-181.
28. Buttlar, W.G., Al-Khateeb, G.G., and Bozkurt, D. (1999). Development of a Hollow Cylinder Tensile Tester to Obtain Mechanical Properties of Bituminous Paving Mixtures, *Journal*

of the Association of Asphalt Paving Technologists, 68, pp. 369-403.

29. Al-Khateeb, G. (2001). *Development of a Hollow Cylinder Tensile Tester to Obtain Fundamental Mechanical Properties of Asphalt Paving Mixtures,* University of Illinois at Urbana-Champaign, USA.
30. Kaklis, K.N., Agioutantis, Z., Sarris, E., and Pateli, A. (2005). A Theoretical and Numerical Study of Discs with Flat Edges under Diametral Compression (Flat Brazilian Test), *5th GRACM International Congress on Computational Mechanics*, Limassol, Cyprus.
31. Thornton, C. (1979). Conditions for Failure of a Face-centered Cubic Array of Uniform Rigid Spheres, *Geotechnique*, 29(4), pp. 441-459.